Chemical Engineering Journal 495 (2024) 153000

Contents lists available at ScienceDirect

Chemical Engineering Journal

journal homepage: www.elsevier.com/locate/cej

Reaction engineering for high yield electrosynthesis: Unraveling the impact of reaction conditions and conversion on methanol oxidation to formate

Jonas Baessler, Niklas Vollmert, Jan Vehrenberg, Miriam Mineur, Sophia Schenke, Lukas Griesberg, Paulina Montero Pineda, Robert Keller *

Chair for Chemical Process Engineering, RWTH Aachen University, Forckenbeckstr. 51, 52074 Aachen, Germany

ARTICLE INFO

Keywords:
Selective methanol oxidation
Alternative anodic reaction
Paired electrosynthesis
Co-generation of hydrogen and formate
Hierarchical electrode
Reaction conditions

ABSTRACT

Electrochemical processes offer defossilized alternatives to conventional routes. Key processes, such as hydrogen evolution and electrochemical CO_2 reduction, are typically paired with the anodic oxygen evolution reaction (OER). However, the generated oxygen holds little value and the electrical costs associated with energy-intensive OER pose a significant economic barrier. The methanol oxidation reaction (MOR) to formate is a promising alternative to OER, requiring less energy and providing a value-added product. Extensive research focuses on MOR regarding high Faraday efficiencies, but conversion and product yields are mostly neglected. However, high conversion with sufficient yield is a prerequisite to transition from lab-scale catalysis towards feasible industrial applications. In this work, we investigated the selectivity of MOR to formate with progressing conversion at high current densities of up to 200 mA/cm^2 on hierarchically structured copper(II) oxide electrodes. We assessed the impact of the reaction conditions, including current density, temperature, flow rate, electrolyte composition, and membrane type. We found a positive influence of low current density and high temperature on the FE. Through tailored reaction conditions, we achieved a formate yield of 70% at 100 mA/cm^2 with an anodic potential of 1.33 V vs. RHE. The anodic potential remained below typical OER potentials even at high conversion. For the first time, we demonstrated that MOR can achieve significant formate yields at high current density. Our results reveal the impact of conversion, reaction conditions and ion balance on selectivity and provide valuable insights for operating MOR at high yield in paired processes, e.g., with hydrogen evolution or CO_2 reduction.

1. Introduction

Anthropogenic carbon dioxide (CO_2) emissions are causing global warming, which severely impacts human life and the ecosystems, if not mitigated [1]. To reduce CO_2 emissions, ongoing efforts are being made to develop sustainable technologies to replace fossil fuels and feedstocks [2]. Electrochemical processes offer promising approaches for the production of chemicals from renewable feedstocks [3,4]. Especially water electrolysis and electrochemical CO_2 reduction (CO2R) have emerged as focal points of extensive research and industrial interest. However, the high cost compared to fossil-based routes presents a major hurdle for both processes [4–6].

Typically, only one half-cell reaction of electrochemical reactors is exploited for the synthesis of value-added chemicals. The value-adding reaction of water electrolysis, CO2R, and various other electrochemical processes is a reduction reaction at the cathode side of the cell. The cathodic reactions typically exhibit low standard potentials, specifically $E^0 = 0$ V vs. standard hydrogen electrode (SHE) for the hydrogen evolution reaction (HER) and $E^0 = -0.1 - 0.2$ V vs. SHE for the CO_2 reduction reaction (CO2RR) to most products [7]. These cathodic reactions are commonly paired with the energy-intensive oxygen evolution reaction (OER) at the anode side, which exhibits a high standard potential of $E^0 = 1.23$ V vs. SHE. Consequently, OER accounts for the majority of the electrical energy demand, while the generated oxygen holds little value and does not contribute to economic viability. The cost of electrical energy is the main contributor to the overall production costs for both water electrolysis and CO2R [4,5]. To reduce the electrical energy demand and enhance economic viability, recent literature has explored replacing the energy-intensive OER with organic oxidation reactions, which can reduce electricity consumption while providing additional value-added products [7–14]. Anodic methanol oxidation to formic acid presents a promising alternative to OER, as it possesses several favorable characteristics: Formic acid (0.64–1.30 $/kg, 29.4–59.8 $/kmol, Table S1) holds higher value compared to methanol (0.34–0.58 $/kg, 10.9–18.6 $/kmol, Table S2)

* Correspondence to: RWTH Aachen University, Aachener Verfahrenstechnik - Chemical Process Engineering, Forckenbeckstr. 51, 52074 Aachen, Germany.
E-mail address: robert.keller@avt.rwth-aachen.de (R. Keller).

https://doi.org/10.1016/j.cej.2024.153000
Received 5 January 2024; Received in revised form 30 April 2024; Accepted 9 June 2024
Available online 15 June 2024

[6,7,15–17]. Moreover, the methanol oxidation reaction (MOR) to formate exhibits a standard potential of 0.1 V vs. SHE, which is significantly lower than the standard potential of OER, indicating its potential to reduce the electrical energy demand [17]. Formic acid and formate salts have a broad range of applications in agriculture, plastics, textile, and pharmaceutical industries [18].

A broad range of catalysts have been developed and investigated for the electrochemical oxidation of methanol to formate with promising results: High Faraday efficiencies (FE) close to 100% and potentials lower than for typical OER have been reported [17,19–24]. MOR has been paired successfully with HER to achieve a more efficient water electrolysis [20–24] and was paired with CO2R to formate in a concurrent synthesis, which generates formate at both the cathode and anode [17,19]. These findings indicate great potential of MOR as an alternative anode reaction to replace OER. However, the achieved formate concentrations were either low or not reported in previous works. Neither the influence of an increasing product concentration has been yet investigated, nor the impact of reaction conditions, ion balance, or water transport. Low formate concentrations are associated with significant costs of downstream processing [25] as the aqueous alkaline formate solution typically employed in MOR requires further purification to formate salts or formic acid. To proceed from the promising lab-scale results to an industrial application, it is crucial that MOR performance is investigated at high methanol conversion , considering the effects that arise with process intensification and increasing formate concentration.

In this work, we investigate the sensitivity of the FE towards methanol conversion in a flow cell at high current densities of up to 200 mA/cm^2. Further, we analyze the effect of different reaction conditions by closely monitoring the reaction via Fourier-transform infrared spectroscopy (FTIR) at a high sampling rate. As a catalyst, we used copper(II) oxide (CuO) on copper foam in the form of a flow-through electrode, which has a very high surface area due to its hierarchical structure over multiple length scales. The impact of the current density, temperature, volume flow, and electrolyte composition on FE and obtainable conversion is investigated and discussed. Furthermore, we assess the influence of different types of ion exchange membranes and investigate how the ionic balances affect the pairing of MOR with cathodic reactions, especially CO2R and HER. Finally, we applied the insights on the reaction conditions to tune the selectivity of MOR, reaching a maximum formate yield of 70% at 100 mA/cm^2 with an anode potential of 1.33 V vs. RHE. In addition, the change in electrolyte volume is quantified and the implications of the water balance are discussed for paired processes at high conversion. Our results reveal the impact of conversion and reaction conditions on the FE and provide insights for operating MOR at high current density and high conversion in paired processes.

2. Material and methods

2.1. Anode preparation and characterization

The preparation of the anode was adapted with modifications from Huan et al. [26,27], using copper foam instead of a copper plate as substrate. Copper foam of 2 mm thickness with 90 pores per inch (POROFEN-Cu90, AlCarbon) was ultrasonically cleaned in acetone for 20 min. An area of 5 × 5 cm^2 of the cleaned copper foam was immersed into a solution of 0.2 mol/L $CuSO_4$ and 3 mol/L H_2SO_4 at 60 °C . Details on the chemicals and materials used in this work are provided in the Supporting Information (Table S3 and S4). A mixed metal oxide coated titanium sheet (Magneto Special Anodes) was used as the counter electrode. Copper dendrites were deposited onto the copper foam at a high current density of 1500 mA/cm^2 provided by a power supply (HMP4040, Rohde & Schwarz) for 60 s, corresponding to a charge of 90 C/cm^2. The solution was not stirred during deposition, as the copper coating was more homogeneous if the solution was only agitated by the gas evolution at both electrodes. After deposition, the foam was thoroughly cleaned with DI water and dried at room temperature. Subsequently, the foam was heated in an oven to oxidize the copper surface to copper(II) oxide (CuO). Starting from 25 °C, the temperature in the oven was increased at a rate of 10 °C/min up to the final temperature of 300 °C, which was maintained for additional 30 min. The electrode structure was examined with a field-emission scanning electron microscope (SEM)(SU5000, Hitachi). Photographs, SEM images, and further characterization of the electrode by energy dispersive X-ray spectroscopy (EDX) and X-ray diffraction analysis (XRD) are provided in the Supporting Information (Figures S1–S3). The settings for the ECSA measurement via double layer capacitance were adapted from Li et al. [28].

2.2. Electrochemical measurements

All electrochemical measurements were carried out in a flow cell with an active area of 5 × 5 cm^2 (flex-E-cell, FXC Engineering) connected to a potentiostat (VSP with 10A booster, Biologic). Potentials were measured using a reversible hydrogen electrode (RHE)(Hydroflex, Gaskatel). The cell setup used for all experiments regarding the impact of the reaction conditions is shown in Fig. 1a. A detailed illustration of the cell configuration is available in the Supporting Information (Figure S4). Two layers of copper foam coated with CuO dendrites as described in ‘Anode preparation’ were used as anode and a platinum (Pt) coated titanium sheet as cathode (Magneto Special Anodes). Unless stated otherwise, the anode was reused within each series of experiments regarding one reaction condition parameter. Degradation of the anode was investigated by conducting electrolysis at each parameter setting in duplicate, first in ascending, then in descending order (e.g. 25 °C, 40 °C, 55 °C, 55 °C, 40 °C, 25 °C). If not specified otherwise, electrolysis was performed at a constant current density of 200 mA/cm^2, a temperature of 25 °C, a flow rate of 50 mL/min of both electrolytes, with 2 mol/L potassium hydroxide (KOH) and 1 mol/L methanol as anolyte, 2 mol/L potassium hydrogen carbonate as catholyte and a bipolar membrane (BPM) (Fumasep FBM-PK, Fumatech). The BPM was operated in reverse bias. As alternative membranes a cation exchange membrane (CEM)(Nafion 212, Chemours) and an anion exchange membrane (AEM)(Fumasep FAA-3-50, Fumatech) were used.

The electrolytes were recirculated with a peristaltic pump (Masterflex L/S Digital, Cole-Parmer) through the electrochemical flow cell and heat exchanger (flex-H-cell, FXC Engineering) for temperature control. The total anolyte volume was 54.5 mL. A detailed description of the experimental setup including a schematic flow sheet is provided in the Supporting Information (Figure S5). For the demonstration of a paired synthesis, the cell setup was changed to reduce the cell potential and a second reference electrode was placed in the catholyte. A nickel mesh (aperture width 0.5 mm, wire diameter 0.14 mm, Haver & Boecker) supported by copper foam was used as cathode as shown in Fig. 1b with 1 mol/L KOH as catholyte.

2.3. Product analysis and evaluation

A sample stream from the anolyte was circulated with a peristaltic pump (Reglo ICC, Ismatec) at 10 mL/min through the flow cell probe of a FTIR spectrometer (ReactIR 702L with Micro Flow Cell, Mettler Toledo). The concentrations of methanol, formate, and OH^- during electrolysis were measured by the FTIR spectrometer at a sample rate of 1 sample per 30 s. Detailed information on the FTIR analysis is provided in the Supporting Information (Figure S6–S7). The concentration data obtained from the ReactIR software was further processed and analyzed in Origin (OriginLab). Weighted adjacent averaging with a window size of 20 points was applied to the concentration data, which smoothed the data without altering the shape of the curves. Methanol conversion,

FE, and formate yield were calculated from the smoothed concentration data according to the following equations:

$$conversion = \frac{c^0_{\mathrm{MeOH}} - c^n_{\mathrm{MeOH}}}{c^0_{\mathrm{MeOH}}} \cdot 100\% \quad (1)$$

$$FE = \frac{zFV}{I} \cdot \frac{c^n - c^{n-1}}{t^n - t^{n-1}} \cdot 100\% \quad (2)$$

$$yield = \frac{c^n_{\mathrm{HCOO-}}}{c^0_{\mathrm{MeOH}}} \cdot 100\% \quad (3)$$

where c is the concentration of the regarding substance and the indices denote the start of the experiment (index 0), the current data point (index n) and the previous data point (index n - 1). z is the number of electrons transferred per reaction, F the Faraday constant, V the anolyte volume, I the current, and t the time.

3. Results and discussion

3.1. Anode characterization

For the present study, copper dendrites were electrodeposited onto an open-cell copper foam at high current density and were subsequently oxidized by a heat treatment in air. After oxidation the color of the electrode changed from red to black, indicating an oxidation to CuO [29]. The oxidation of the electrode and the presence of Cu_2O and CuO were confirmed by EDX and XRD measurements (Figure S3). The black color of the electrode and the presence of both Cu_2O and CuO were consistent with previous studies that found a multilayer oxide structure of dendritic copper oxide electrodes, with copper at the core, covered by a layer of Cu_2O, followed by an outer layer of CuO [26,30]. Fig. 2 shows SEM images of the copper oxide electrode at four different magnification levels. The open-cell structure of the foam substrate provides large pores, allowing electrolyte flow through the 3D-structured electrode (Fig. 2a). The pore diameter of the untreated foam is 730 µm ± 60 µm, which narrows slightly due to the growth of the dendrite layer. The dendrite layer has a cratered surface, caused by hydrogen bubbles during electrodeposition. The craters of the dendrite layer have a diameter of about 50 µm (Fig. 2b). The deposited dendrite layer features a porous fractal-like structure with interconnected branches of 0.1–10 µm thickness (Fig. 2c). The surface of the oxidized dendrites exhibits roughness down to the nanometer scale (Fig. 2d). The electrode features a hierarchical structure with porosity and surface morphology on multiple length scales, thus providing a large surface area for electrochemical reactions. The electrochemical active surface area (ECSA) of the oxidized foam electrode with the deposited dendrite structure was nearly 400 times higher compared to a flat CuO sheet (Figure S8).

The prepared hierarchical CuO anode was active for OER and MOR as illustrated in the LSV curves in Fig. 3. At a potential of 1.59 V vs. RHE, a current density of 100 mA/cm^2 was reached for OER in 2 mol/L KOH. The OER activity of the prepared anode was comparable to state-of-the-art non-noble metal OER catalysts [31,32]. The potential of MOR in 2 mol/L KOH + 1 mol/L methanol reached 100 mA/cm^2 at 1.37 V vs. RHE, which is significantly lower than the potential required for typical alkaline OER [31,32]. However, compared to the standard potential of MOR, the overpotential was still high. A similar or higher overpotential for MOR was observed in previous works with non-noble metal electrodes as well [17,19–22,24], indicating the need for further improvements to reduce the energy demand of MOR.

3.2. Impact of conversion

The time-dependent concentrations of methanol and formate during methanol oxidation with the prepared CuO anode are illustrated in Fig. 4a. The decrease of the methanol concentration was nearly linear over time, resulting in a linearly increasing conversion, which was

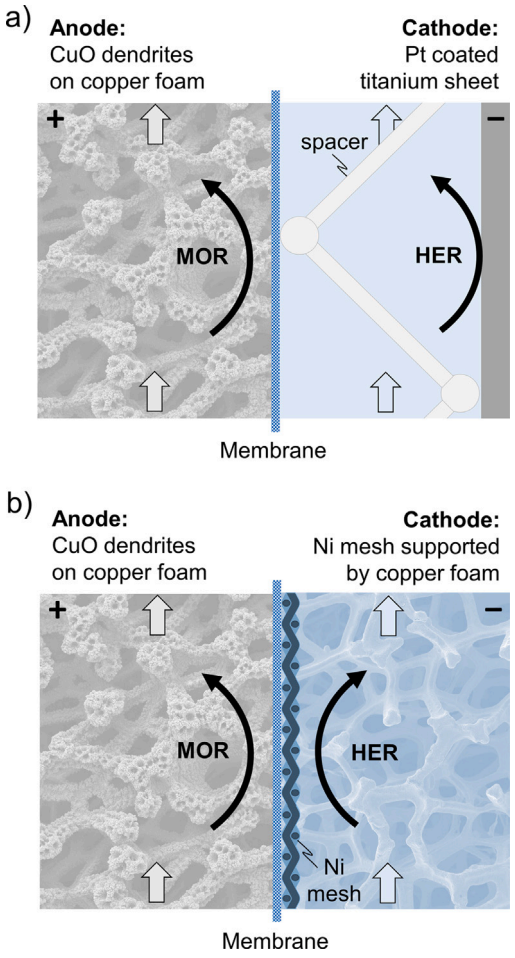

Fig. 1. (a) Schematic of the cell setup used for all experiments regarding the impact of the reaction conditions and (b) cell setup without electrolyte gap for demonstration of paired synthesis.

calculated from the methanol concentration by Eq. (1). In contrast to the linear course of methanol, the formate concentration increased with a decreasing slope to a maximum concentration of 0.42 mol/L. Based on the absence of unidentified substances in the FTIR and additional HPLC analysis of the anolyte, we conclude that all methanol that was not converted to formate was further oxidized to carbonate.

Consistent with our conclusion, we observed that the carbonate peak increases with increasing conversion in the FTIR spectrum (Figure S6). Unfortunately, we were not able to reliably quantify the carbonate peak, as it strongly overlapped with a second formate peak. However, we tested our conclusion in regard of the carbon and charge balance of the anolyte. If carbonate is the only side product of MOR, the carbonate concentration can be determined by calculating the difference between the consumed methanol and the produced formate. Fig. 4a depicts the carbonate concentration calculated from this difference as a dashed line. The FEs of formate and carbonate calculated from the concentration curves by Eq. (2) add up to nearly 100% over the entire experiment as shown in Fig. 4b. Please note that the FE is plotted over the methanol conversion instead of the reaction time. The representation of FE as a function of the conversion allows a more straightforward comparison of experiments with different initial reactant concentrations, current densities, and electrolyte volumes. The FE sum of approximately 100% (103% on average) shows that the balances of carbon and charge are closed providing a strong indication of no further side reactions. Other possible side reactions would have resulted in detectable products and do not match the balances of charge and carbon which indicate

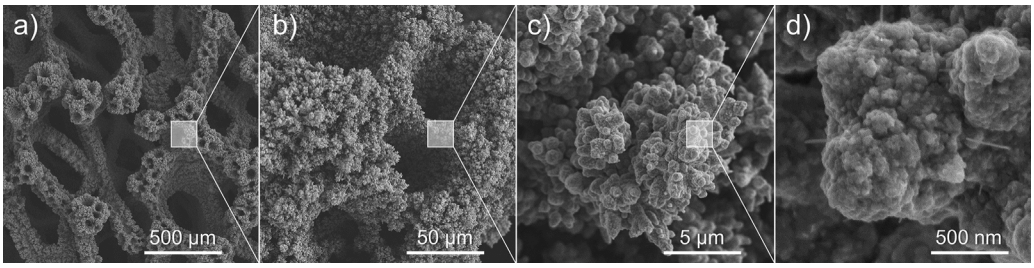

Fig. 2. SEM images of the prepared anode at four different magnification levels of ×50, ×500, ×5k and ×50k (a–d).

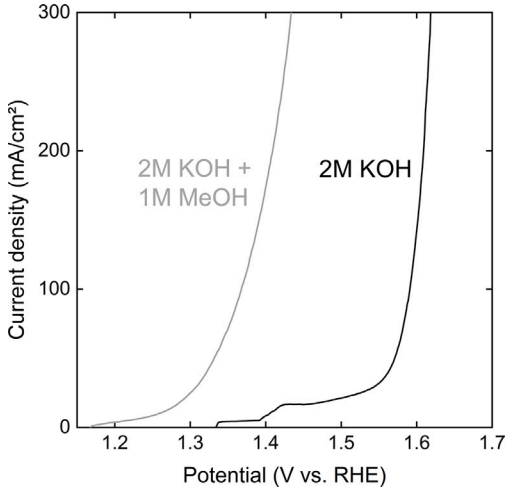

Fig. 3. LSV curves (iR-drop compensated) of the prepared CuO anode measured at a sweep rate of 5 mV/s in 2 mol/L KOH (OER) and 2 mol/L KOH with 1 mol/L methanol (MOR).

a transfer of about six electrons per methanol consumed that was not converted to formate. Therefore, the closed balances justify the assumption of carbonate formation as the only notable side reaction which is consistent with previous studies on alkaline methanol oxidation to formate on copper-based electrodes [17,33]. The formate FE initially reached 85% but decreased significantly with increasing conversion — reaching zero at 74% conversion, while the carbonate FE increased from less than 20% up to 100%. The course of the FE indicates that methanol oxidation to formate (Eq. (4)) competed with carbonate formation. Heli et al. proposed a mechanism for methanol oxidation on copper in alkaline solution, which involves the formation of a Cu^{III} species, which catalyzes the oxidation of methanol and its intermediates to formate or carbonate [33]. For the nature of the Cu^{III} entity, copper oxy-hydroxide (CuOOH) and a Cu^{III} radical (CuOO•H) were proposed [33–36]. Based on the course of the FE, we hypothesize that carbonate was formed in two different pathways as was found for MOR on NiOOH [37]: further oxidation of formate to carbonate (Eq. (5)) and methanol oxidation to carbonate (Eq. (6)). Methanol was initially present in high excess, whereas, at the end of the experiment, the concentration of formate was more than two times higher than the concentration of methanol. The increasing ratio of formate to methanol favors formate oxidation over formate formation, which is a plausible explanation for the decrease in formate FE with increasing conversion. The low initial carbonate formation at near-zero formate concentrations indicates that formate is the preferred product of methanol oxidation.

$$CH_3OH + 5OH^- \longrightarrow HCOO^- + 4H_2O + 4e^- \quad (4)$$

$$HCOO^- + 3OH^- \longrightarrow CO_3^{2-} + 2H_2O + 2e^- \quad (5)$$

$$CH_3OH + 8OH^- \longrightarrow CO_3^{2-} + 6H_2O + 6e^- \quad (6)$$

It should be noted that the pathway of carbonate formation does not change the overall result from an application perspective, as it does not affect the overall carbon and charge balance. The overall reaction scheme for the superposition of methanol oxidation to formate and simultaneous formate oxidation to carbonate is identical to the full oxidation of methanol to carbonate (Eqs. (4)+(5) = (6)). Further information on the reaction mechanism and side reactions is provided in the Supporting Information (Section S9).

3.3. Impact of the reaction conditions

To investigate the impact of the reaction conditions on MOR and to optimize the reaction for high formate yield at high conversion, current density, temperature, flow rate, electrolyte composition and the type of ion exchange membrane were systematically varied. Fig. 5a presents the FE plotted over conversion for three distinct current densities: 50, 100, and 200 mA/cm^2. With decreasing current density, the FE for formate increased and higher conversions were achieved before the FE declined to zero. At a current density of 50 mA/cm^2, a maximum FE of 92% and a conversion of 88% were achieved, in contrast to 85% FE and 78% conversion at 200 mA/cm^2. The relationship between FE and current density was nonlinear in our experiments. The increase in FE from 200 to 100 mA/cm^2 was approximately equal to the increase in FE from 100 to 50 mA/cm^2. The decreasing FE with increasing current density hints towards mass transfer limitation. The local concentration of formate within the porous dendrite layer is expected to rise as the current density increases, while the local concentration of methanol decreases correspondingly. The higher ratio of educt to product facilitates the selectivity of methanol oxidation to formate at a lower current density.

Fig. 5b illustrates the impact of temperature on the FE over conversion. With increasing temperature, the FE for formate increased, and higher conversions were achieved before the FE declined to zero. Specifically, at a temperature of 55 °C, a maximum FE of 93% and a conversion of 83% were attained, whereas at 25 °C, the FE and conversion were slightly lower, at 83% and 74%, respectively. Despite an increased fluctuation of the results at 25 °C, the positive effect of higher temperatures on FE is evident. With increasing temperature, more formate and less carbonate were formed. Higher temperatures could directly affect selectivity by either altering the reaction kinetics or by improved mass transport. We assume a significant contribution of the improved mass transfer, as we expect diffusion coefficients to increase approximately two-fold over the investigated temperature range of 25–55 °C [38,39]. The improved mass transfer increases both the rate at which methanol is transported from the bulk electrolyte to the electrode surface and the rate at which formate is transported in the opposite direction. Hence, an improved mass transfer increases the concentration ratio of methanol to formate at the electrode surface, which increases selectivity towards formate.

Interestingly, the flow rate of the electrolyte through the foam anode had no significant effect on the FE as shown in Fig. 6a for flow rates of 100, 50 and 25 mL/min. A higher flow rate increases the convective mass transport to the electrode surface [40], which typically improves

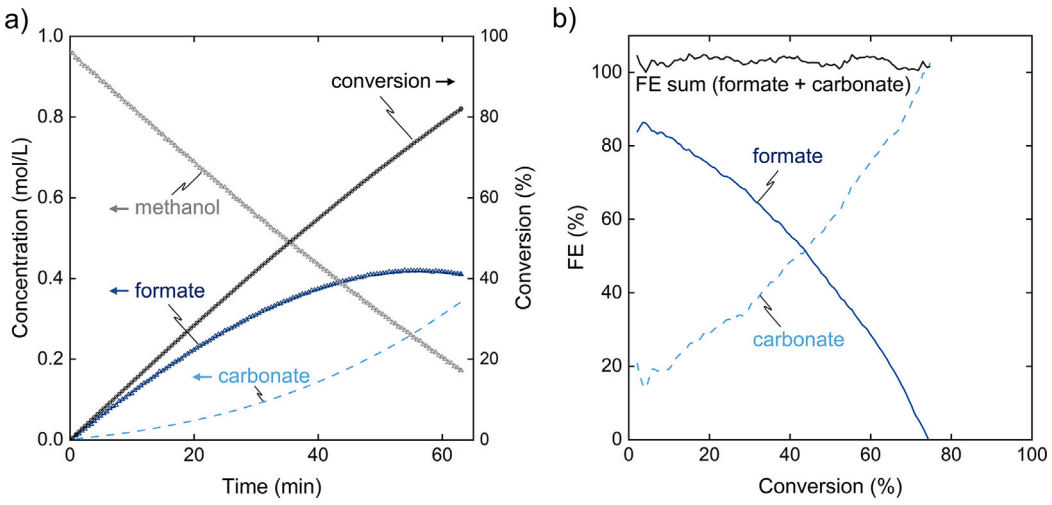

Fig. 4. (a) Concentration of methanol (gray) and formate (blue) measured by the FTIR online analytics during an oxidation experiment at 200 mA/cm^2. The conversion (black) was calculated from the methanol concentration. The carbonate concentration (light blue, dashed) was calculated from the difference of methanol and formate concentration based on the assumption of carbonate being the only side product. (b) The sum of formate and carbonate FE (black), the formate FE (blue) and the carbonate FE (light blue, dashed) were calculated from the concentration data.

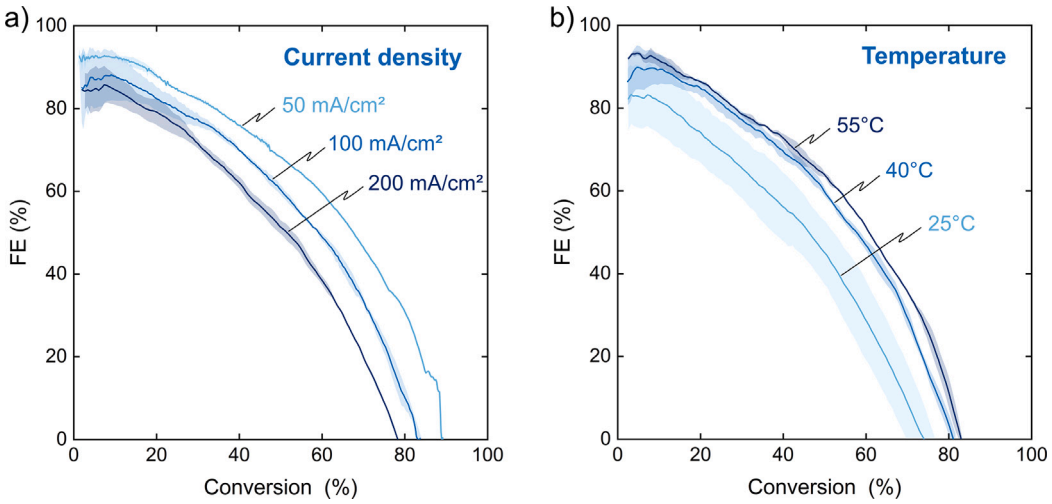

Fig. 5. (a) FE for formate plotted over the conversion of methanol for three different current densities. (b) Influence of the anolyte temperature on the FE to formate over increasing methanol conversion. The mean FE (continuous line) and the range of the replicates (boundaries of the filled area) are shown. If not stated otherwise in the plot, the oxidation was conducted at 200 mA/cm^2, 25 °C, 50 mL/min, 2 mol/L KOH, 1 mol/L methanol and with a BPM.

the selectivity at higher current density, as concentration gradients from the bulk electrolyte to the electrode surface are mitigated [41].

We hypothesize that the flow rate had no significant influence on the FE due to a combination of multiple effects: We expect convective flow through the macroscopic pores of the open-cell copper foam (pore size of about 500 μm), but mainly diffusive transport in the porous dendrite layer due to the small pore size between the dendrites of about 1–10 μm. The assumed mass transport is illustrated in the qualitative schematic of concentration gradients in Fig. 6b. The flow rate can affect the convective transport from the bulk electrolyte to the surface of the dendrite layer, reducing the thickness of the concentration boundary layer. However, the diffusive transport resistance of the porous dendrite layer would remain unaffected, thus reducing the overall effect of the flow rate. Furthermore, the rear areas of the electrode were likely less affected by mass transfer as the local current density is expected to decrease with increasing distance from the membrane due to the increasing electrolyte resistance. Finally, the mass transfer in flow-through foam electrodes increases sublinear with increasing flow rates. Cognet et al. [42] found that the relationship between the mass transfer coefficient k and the flow velocity u is $k \sim u^{0.42}$ for a similar foam electrode with 100 pores per inch. Assuming that the same relationship can be applied to our electrode, increasing the flow rate by 100% would increase the mass transfer coefficient only by 34%. As the relationship between the mass transfer coefficient and FE is presumably sublinear as well, we expect that the FE is even less influenced by the flow rate. Thus, a combination of the described effects seems to reduce the impact of the flow rate on the FE to an extent below significance.

Fig. 7a depicts the relationship between FE and conversion for three distinct concentrations of KOH (1, 2, and 4 mol/L). At low conversion, a higher KOH concentration led to a decrease in FE. We assume that the higher OH^- concentration facilitates the undesired side reactions resulting in full oxidation to carbonate, as the side reactions (Eqs. (5) and (6)) require more OH^- per electron than the partial oxidation of methanol to formate (Eq. (4)). Specifically, an initial FE of 91% was attained at 1 mol/L KOH, compared to 65% when a KOH concentration of 4 mol/L was used. However, as the conversion increased, the FE declined steeper with 1 mol/L KOH, reaching 0% FE at a lower conversion compared to the higher KOH concentrations. We hypothesize that the FE declined more pronounced with 1 mol/L KOH because a minimum concentration of OH^- ions is required for selective oxidation of methanol to formate at CuO.

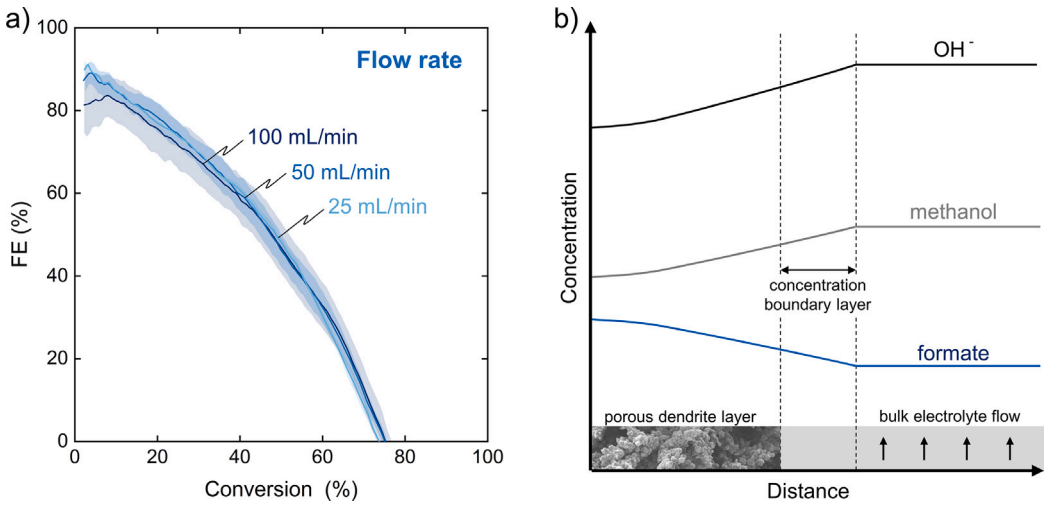

Fig. 6. (a) Influence of the flow rate on the FE to formate over increasing methanol conversion. The mean FE (continuous line) and the range of the replicates (boundaries of the filled area) are shown. The oxidation was conducted at 200 mA/cm^2, 25 °C, 2 mol/L KOH, 1 mol/L methanol, with a BPM. (b) Qualitative schematic of the concentration gradients at the electrode surface.

At least 5 OH^- ions are consumed per oxidized methanol (Eq. (4)), while up to 4 OH^- ions can be compensated by ion transfer to the anolyte (see Fig. 8c). In total, at least one OH^- ion is depleted per oxidized methanol. Thus, an initial concentration of 1 mol/L KOH is not sufficient to completely convert 1 mol/L methanol without a significant drop in pH. Fig. 7c depicts the decreasing KOH concentration in the anolyte during methanol oxidation to formate. While the rate of KOH consumption was similar, the rate was not identical for the different initial KOH concentrations. The slope of the KOH concentration was slightly steeper at high initial KOH concentration and low formate FE, which is in good agreement with the theoretical rates of KOH consumption determined from the ion balances. The ion balances result in slightly different rates of KOH consumption of 0.33 vs. 0.25 KOH consumed per electron transferred for methanol oxidation to carbonate vs. methanol oxidation to formate (Figure S10). In the experiments with 1 mol/L KOH the concentration of KOH decreased to 0.29 mol/L at the point of zero FE. The local OH^- concentration at the electrode surface was likely lower than the measured bulk concentration, as pronounced concentration gradients as shown in Fig. 6 are expected at high current density. To avoid a steep decline of the FE, the amount of KOH should be chosen such that a sufficient excess of OH^- remains at high conversion. In future studies, adding KOH continuously or stepwise could counter the neutralization of OH^- caused by the formate formation and maintain an optimal pH.

Fig. 7b illustrates the effect of methanol concentration on the FE over progressing conversion with three different initial methanol concentrations (2, 1, and 0.5 mol/L). Initially, a maximum FE of 92% was observed with 2 mol/L methanol, in contrast to the 71% achieved with 0.5 mol/L. In general, higher methanol concentrations resulted in higher FE for formate. The ratio of methanol to formate at a given percentage of conversion was similar, independent of the initial methanol concentration. We attribute the increased FE to the higher absolute methanol concentration and to the associated higher mass transport of methanol to the electrode, which likely facilitates methanol oxidation to formate. However, at high conversion, the FE decreased more pronounced with 2 mol/L methanol, than at lower initial methanol concentrations.

The sharp drop of the FE with 2 mol/L methanol and 2 mol/L KOH is similar to the experiment with 1 mol/L methanol and 1 mol/L KOH (see Fig. 7a). As discussed in the previous paragraph, we assume that the FE decreases strongly when the OH^- concentration in the electrolyte becomes too low and the local reaction environment at the electrode surface becomes too acidic. Fig. 7d shows the KOH concentration plotted versus conversion for the experiments with different methanol concentrations. In the experiment with 2 mol/L methanol and 2 mol/L KOH, the sharp drop of the FE occurred when the KOH concentration was low. The KOH concentration declined down to 0.35 mol/L at the end of the experiment. The initial ratio of methanol to KOH of 1:1 was too low to maintain a sufficient OH^- concentration at high methanol conversion.

Fig. 8a illustrates the impact of the membrane type on the FE. The BPM exhibited the highest initial FE of 76%, followed by the CEM with 57%, and the AEM with 36%. With progressing conversion, the FE decreased for all tested ion exchange membranes. In contrast to all other reaction conditions tested, we observed clear indications of corrosion of the CuO electrode at the end of the MOR experiments with the AEM and the CEM. A blue hue was visible in the anolyte indicating dissolved copper ions and the electrode color changed partially from black (CuO) to copper (metallic Cu). Therefore, a new anode was used for each membrane experiment. We attribute the corrosion of the CuO electrode to the less favorable ion balance of the AEM and CEM causing a reduced local pH at the membrane electrode interface, which is discussed in more detail in the subsequent paragraphs.

The choice of ion exchange membrane significantly influences the ion transport through the membranes and thus, the overall ion balance. Fig. 8b shows the KOH concentration decreasing over time. The decline in KOH concentration occurred at a substantially slower rate with a BPM compared to a CEM or AEM. The distinct slopes observed for the KOH concentration over time can be attributed to the different ion balances of the three membrane types (Fig. 8c–e). In the case of the BPM, the reaction of methanol to formate consumes 5 OH^- ions, while 4 OH^- ions are supplied to the anolyte through ion transfer resulting from water dissociation in the BPM.

When employing a CEM, the charge transport across the membrane relies on the transfer of K^+ ions from the anolyte to the catholyte. Consequently, the consumption of OH^- ions is not compensated by ion transfer through the membrane as it is with a BPM. As a result, the ratio of OH^- ions consumed per electron transferred is considerably higher in a CEM compared to a BPM. The observed decline in KOH and OH^- concentration is in good agreement with the OH^-/e^- ratio of −1.25, resulting from the ion balance of the CEM. The lower conversion achieved with a CEM is likely caused by the rapid decline in OH^- concentration. Although a concentration of 0.23 mol/L OH^- remained in the bulk electrolyte at the end of the experiment, the OH^- concentration in the porous dendrite layer of the anode is expected to be significantly lower. Corresponding to the experiments with lower KOH concentration the

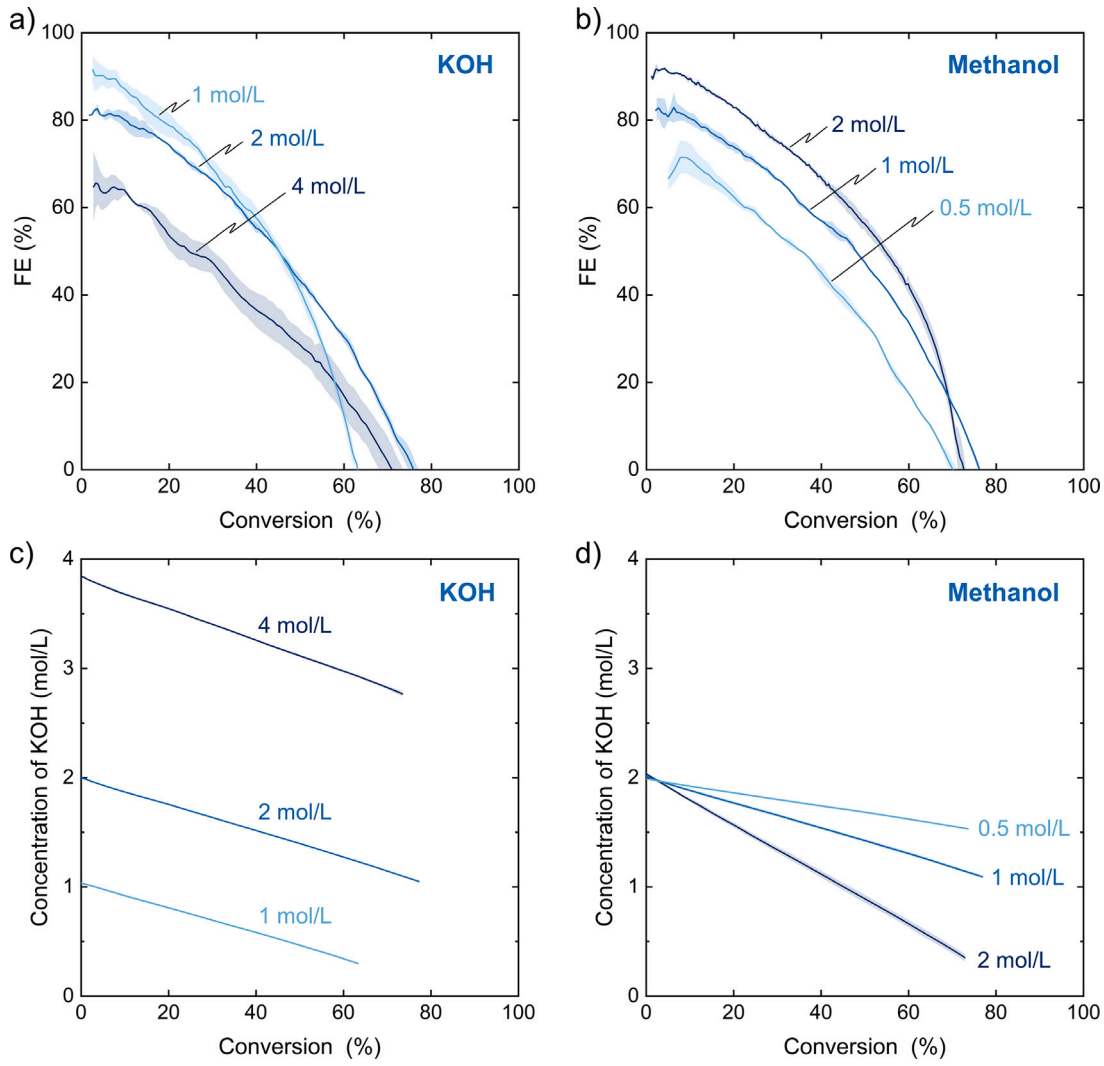

Fig. 7. (a) Influence of the initial KOH concentration and (b) of the initial methanol concentration on the FE to formate. (c–d) KOH concentration in the same experiments plotted over methanol conversion. The mean FE and the mean KOH concentration (continuous lines) are shown along with the range of the replicates (boundaries of the filled area). If not stated otherwise in the plot, the oxidation was conducted at 200 mA/cm^2, 25 °C, 50 mL/min, 2 mol/L KOH, 1 mol/L methanol, with a BPM.

quickly declining FE at low OH^- concentration indicates that a low pH impedes methanol oxidation to formate. Interestingly, the initial FE was lower with a CEM or AEM compared to a BPM even before the different KOH concentration of the bulk electrolyte is expected to have a significant impact. This observation can be attributed to the local reaction conditions in the region of the electrode, which is adjacent to the membrane and therefore directly impacted by the membrane transport. As stated above, the part of the anode directly adjacent to the membrane will be the most active. Due to the iR drop, electrode segments at a greater distance to the membrane will be less active.

When using an AEM, the anions in the catholyte determine the ion transfer across the membrane. We have used $KHCO_3$ in the catholyte to mimic the conditions of electrochemical CO2R. We expect that most of the charge transport across the membrane occurs via the transfer of HCO_3^- ions and that each HCO_3^- transported neutralizes another OH^- for conversion to CO_3^{2-} in the highly alkaline anolyte, as shown in the ion balance (Fig. 8e). The measured decline in the KOH and OH^- concentration is more pronounced with an AEM compared to a CEM. However, the slope of the measured decline is less negative than the OH^-/e^- ratio of −2.25 derived from the ion balance for the AEM. This suggests that additional ions may be transported across the membrane, potentially mitigating the decrease in OH^-. It is plausible that CO_3^{2-} and OH^- were involved to some extent in the charge transfer across the AEM, despite their low concentration in the catholyte. As we will show, a different catholyte composition changes the ion balance for the AEM. With regard to a stable pH in the anolyte, the transport of OH^- as the only anion across the membrane is ideal. For common catholytes of alkaline water electrolysis, such as KOH or NaOH, we do not expect any difference in the ion balance between AEM and BPM.

In addition to the ion transfer required for charge transport, other transport phenomena across the membrane should be considered as well. The crossover of methanol and formate through the membrane to the cathode side can cause the loss of reactant and product or negatively affect the catholyte reaction. We analyzed the catholyte after the oxidation experiments with the three different membrane types via HPLC (Table S5). There was no significant crossover of methanol or formate through the BPM. The CEM retained the negatively charged formate but was permeable to uncharged methanol. Methanol can pass through the CEM by diffusion driven by the concentration difference, but also by electroosmotic drag along with the transported cations [43]. The AEM was permeable to formate and methanol, which can both diffuse through the membrane driven by the concentration difference.

Besides the influence on FE and conversion, the reaction conditions also affect the potential of the anode. Fig. 9 compares the mean anodic potential during methanol oxidation at different reaction conditions. Typical chronopotentiometry curves are provided in Figure S11. The

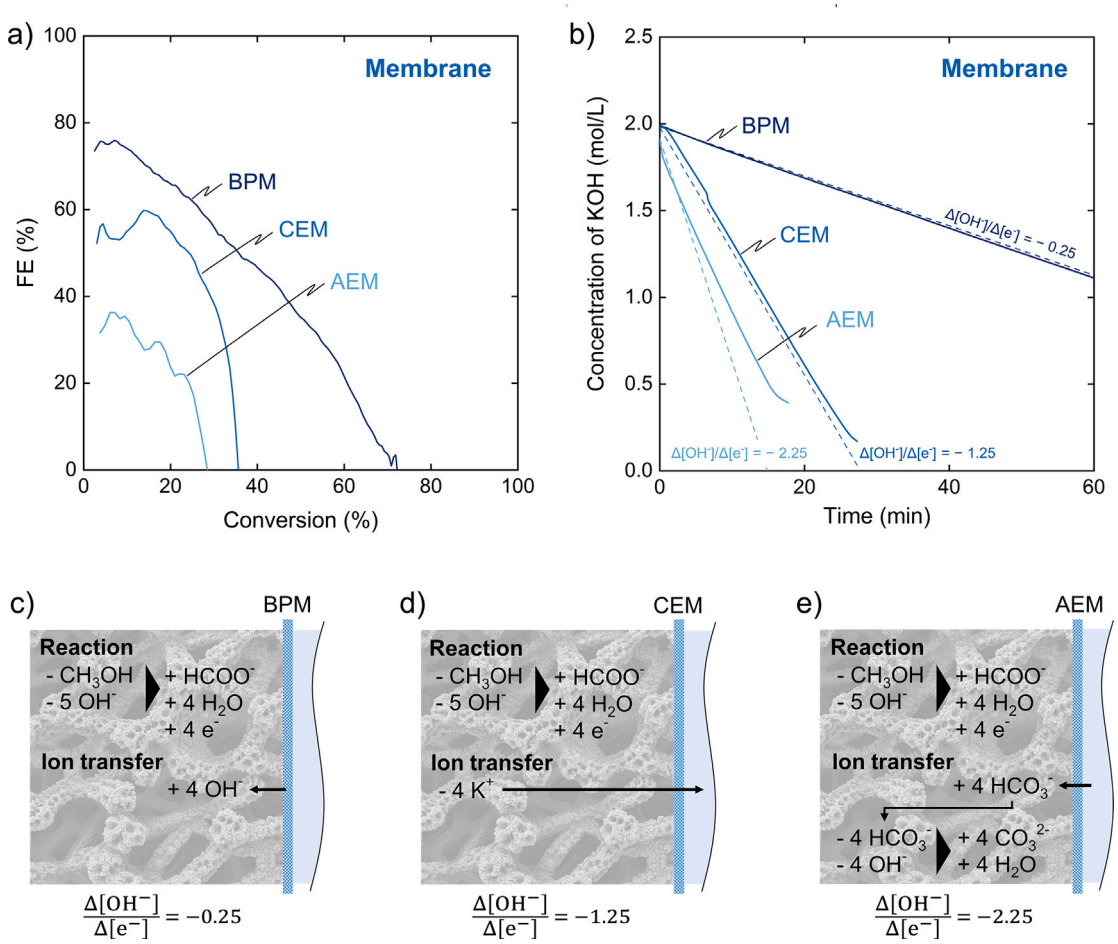

Fig. 8. (a) Influence of the membrane type on the FE to formate over increasing methanol conversion. The oxidation was conducted at 200 mA/cm^2, 25 °C, 50 mL/min, 2 mol/L KOH and 1 mol/L methanol.(b) Decreasing KOH concentration during the experiments (continuous line). Calculated concentration curves (dashed line) for the theoretical ratios of OH^- consumption per electron transferred are shown for comparison. (c)–(e) Balances of the anode side considering methanol oxidation to formate and ion transfer through the different membrane types. Based on the balances, theoretical ratios of OH^- consumption per electron transfer are given.

anodic potential increased significantly with increasing current density (Fig. 9a), which we attribute primarily to the increasing voltage drop across the resistance of the electrolyte. The electrolyte gap to the membrane was minimized as the foam electrode was placed in direct contact with the membrane. However, it should be noted that the electrolyte conductivity can still have a significant effect on the local potential distribution within the foam electrode. The potential decreased slightly with increasing temperature (Fig. 9b), which is due to improved kinetics and electrolyte conductivity. A quantitative relationship between temperature on the overall reaction rate is provided by an Arrhenius plot in the Supporting Information (Figure S12). The flow rate had no clear effect on the potential (Fig. 9c). The potential decreased with increasing KOH concentration and the corresponding higher electrolyte conductivity (Fig. 9d). The influence of the methanol concentration on the potential was small in the investigated concentration range. The results suggest a slightly higher potential at higher methanol concentration (Fig. 9e), which agrees with a lower conductivity expected at higher methanol concentration [44]. The membrane had no significant effect on the anodic potential (Fig. 9f). It should be noted that the experiments with the CEM and AEM were not performed in duplicate due to the corrosion of the CuO electrode (see discussion of Fig. 8).

While the duration of use showed no clear effect on the FE, we observed an increase in the anodic potential from experiment to experiment at high current density and low temperature. We observed no increase in potential between the experiments when the anode was operated at low current density or high temperature. Considering both anodic potential and FE for formate, three parameters (current density, KOH concentration, and methanol concentration) presented a trade-off between electrical energy demand and product selectivity. However, an increased temperature improved both anodic potential and FE.

3.4. High yield MOR at tuned conditions & considerations for paired synthesis

To demonstrate a paired synthesis with high-yield MOR, we paired MOR in two different setups with alkaline HER utilizing the insights gained from our investigation of the reaction conditions. The two setups depicted in Fig. 10a–b employ different membranes and electrolyte management creating opposite characteristics that will be discussed in the following paragraphs.

The BPM setup with separated electrolytes allows the operation of anodic MOR and a cathodic reaction practically independent of each other. The BPM retains both anions and cations, effectively preventing the exchange of anions or cations between anolyte and catholyte. The OH^- migration to the anolyte mitigates the decreasing pH with progressing conversion as shown in Fig. 8. With these characteristics, we expect the BPM setup to be suitable to pair MOR at high yield with most cathodic reactions, including electrochemical CO2R. Successful operation of CO2R with BPMs was documented with electrolyte gap [45,46] and in zero-gap configuration [47,48].

The AEM setup utilizes a shared electrolyte, which is cycled through the anode and cathode compartments. In contrast to the BPM setup, anodic MOR, and a paired cathodic reaction are not independent of each other as both sides share the same electrolyte. For successful

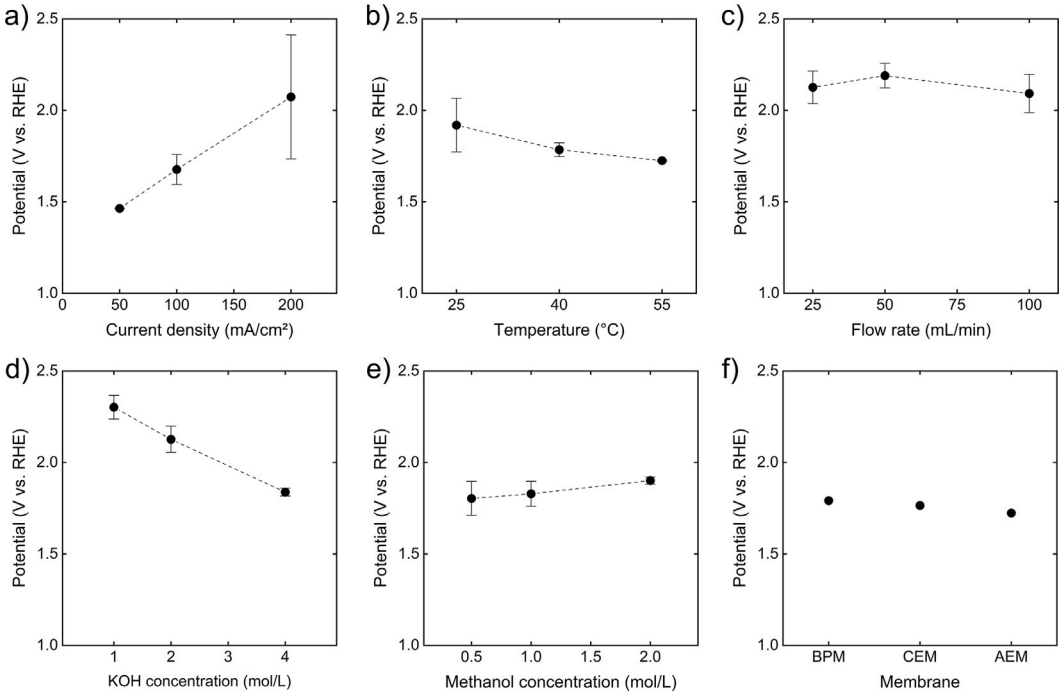

Fig. 9. Mean anodic potential during methanol oxidation at different reaction conditions: (a) current density, (b) temperature, (c) electrolyte flow rate, (d) initial KOH concentration, (e) initial methanol concentration, and (f) membrane. The error bar represents the range of the replicates. If not indicated otherwise by the values of the *x*-axis, the oxidation was conducted at 200 mA/cm^2, 25 °C, 50 mL/min, 2 mol/L KOH, 1 mol/L methanol and with BPM.

pairing, the cathodic reaction must be compatible with the electrolyte of MOR, while MOR must be compatible with the reactants and products of the cathodic reaction. Compatibility implies that the substances in the electrolyte (KOH, methanol, formate, educt, and product of the cathodic reaction) do not undergo undesired reactions or interact negatively with the desired reactions. While the options for compatible cathodic reactions are limited, alkaline HER was successfully paired with MOR in shared electrolyte setups with no negative interactions reported [20–24].

Both setups were operated at a current density of 100 mA/cm^2 with the same reaction conditions, pairing high-yield MOR with alkaline HER. Fig. 10c shows the mean cell potential for the paired synthesis divided into the potentials of membrane, cathode, and anode. The cell potential of the BPM setup was 2.9 V and 1.8 V for the AEM setup. The higher cell potential of the BPM setup was mainly caused by the higher membrane potential of the BPM compared to the AEM setup. BPMs require an additional potential for water dissociation within the membrane [49], the measured membrane potential of 1.08 V was within the manufacturer's specifications of <1.2 V at 100 mA/cm^2. The effective separation of the electrolytes by the BPM came at the cost of a higher cell potential. However, the trade-off between higher potential and improved ionic balance of the separate electrolytes is not a challenge unique to paired synthesis with MOR. For example, BPMs are considered for CO2R despite their higher membrane potential as BPMs can prevent salt formation and increase CO_2 utilization [50]. The cathodic potentials for HER were acceptable for a demonstration of a paired synthesis focused on anodic MOR, but are higher than for state-of-the-art alkaline HER catalysts [32] as the plain nickel mesh used as cathode is not an optimized catalyst. The mean anodic potential was remarkably low with 1.49 V for the BPM setup and 1.33 V for the AEM setup, which is significantly below typical alkaline OER potentials [31,32].

We measured the weight change of the electrolyte to test the hypothesis that the electrolyte volume changes at high conversion. The weight change corresponds to a change in the electrolyte volume as the change in density was neglectable. For the BPM setup the weight of the anolyte increased by 10.7%, while the weight change of the shared electrolyte in the AEM setup was −0.7%. We can exclude that leakage was causing the weight change, as the weight did not change as we operated the setup with running pumps but without current. The slight reduction in electrolyte weight in the AEM setup is most probably due to hydrogen evolution and evaporation since the volatile components of the electrolyte can escape along with the hydrogen gas formed at the cathode. The observed increase of anolyte weight was larger than expected for a symmetrical water balance of the BPM setup (Figure S13), in which the water split in the BPM originates at equal parts from anolyte and catholyte. We attribute the additional weight increase to an asymmetrical water balance, which led to an increased water transport to the anolyte. The asymmetrical properties of BPMs were discussed in previous studies [49,51,52]. A net water transport to the anode side could occur if the water drag of the OH^- ions transferred to the anolyte exceeds the diffusion of water from the anolyte into the membrane. It should be noted that water transport through CEMs or AEMs is typically more pronounced with reported water transfer numbers (moles of water transferred per faraday of electricity) of 2–15 depending on the ionomer, the transferred ion and the humidification of the membrane [53–55]. Our findings highlight that the volume change of the electrolyte and the water balance of the cell should be considered for electrosynthesis at high product concentrations. While the volume change of the electrolyte in the AEM setup was negligible, we took the volume change of the anolyte in the BPM setup into account for the evaluation. In the following, we discuss the impact of the water balance on the practical operation of anodic MOR and its implications on the reaction efficiency. In the BPM setup, the water transport across the membrane dilutes the reactant and product concentration in the anolyte. This dilution of the reactant concentration (methanol) can decrease the selectivity for formate, as our results show that the formate FE decreases with lower methanol concentration (see Fig. 7). From the perspective of downstream processing, a dilution of the product is undesirable, as this is likely connected to increase separation costs. In our case, the observed dilution rate of 10% might be acceptable. Nevertheless, dilution is linked to the amount of charge transferred and will, therefore, increase for higher product concentrations. In contrast

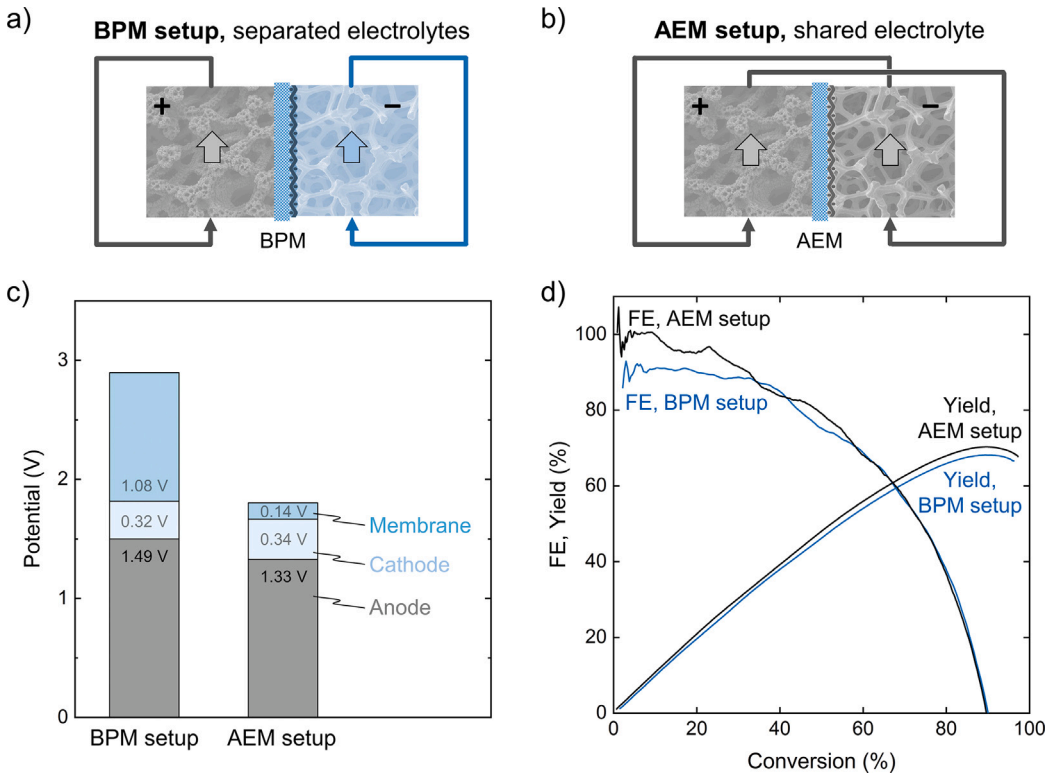

Fig. 10. (a–b) Setups used for paired synthesis of anodic MOR to formate and cathodic HER. (c) Cell potential of both setups divided into the contributions of membrane, cathode, and anode potential. (d) FE and yield of formate plotted over the conversion of methanol for both setups. The oxidation was conducted at 100 mA/cm^2, 55 °C, 50 mL/min, 2 mol/L KOH and 1 mol/L methanol.

to the BPM setup, the water balance of the AEM setup with a shared electrolyte is closed. Hence, water transport does not negatively affect the product concentration in the AEM setup.

Fig. 10d illustrates the FE and the yield for MOR to formate over progressing methanol conversion for both setups. Both setups exhibited a high initial FE of 95%–101% for the AEM setup and 86%–93% for the BPM setup. With increasing methanol conversion the FE of both setups converged, reaching a high conversion of 90% before the FE decreased to zero. Operating MOR at an elevated temperature of 55 °C and a reduced current density of 100 mA/cm^2 showed a higher selectivity compared to applying the settings not in combination as shown in Fig. 5a and b. Both setups achieved high maximum yields of up to 70% for the BPM setup and 68% for the AEM setup. In summary, both setups reached a high FE and formate yield at low anodic potential. The BPM setup is less energy efficient due to the higher membrane potential, but more versatile in pairing with other reactions as the setup can be operated with separated electrolytes. In contrast, the AEM setup is more energy efficient with a low membrane potential, but less versatile. Compatible cathodic reactions are limited to reactions such as HER that can be operated in the shared alkaline electrolyte containing methanol and formate. Our results show that MOR can be operated in both setups at reduced anodic potential compared to OER, while providing formate at high yield as additional value-added product.

4. Conclusion

In summary, we investigated the impact of reaction conditions and conversion on methanol oxidation to formate on a hierarchically structured electrode and demonstrated a paired synthesis at a high formate yield. The hierarchically structured CuO anode exhibited a high surface area with porosity on different length scales from 500 μm to 500 nm and was highly active for methanol oxidation. The reaction progress was monitored with fast sampling analytics, which allowed us to reveal the relationship between FE and conversion. We observed a high initial FE of 85% at 200 mA/cm^2 which declined with increasing slope over the progressing conversion of methanol, reaching 75% conversion before the FE declined to zero. The conversion had a significant impact on the selectivity by changing the ratio of methanol to formate, as methanol oxidation to formate was competing with the subsequent oxidation of formate to carbonate.

Decreasing the current density or increasing the temperature increased both the initial FE and the obtainable conversion before the FE declined to zero. An increased electrolyte flow rate had no significant effect on MOR suggesting that concentration gradients formed mainly inside the porous dendrite layer. Our results on different electrolyte compositions and membrane types highlight the importance of the ionic balance for a stable electrosynthesis at high conversion.

Applying the insights into the reaction conditions, we demonstrated a paired synthesis of cathodic HER and anodic MOR to formate at 100 mA/cm^2 with an initial FE close to 100% reaching a formate yield of up to 70% at 90% conversion. To the best of the authors knowledge, the achieved conversion and yield are the highest values reported so far. The anode potential of 1.33 V vs. RHE for MOR at the hierarchical non-noble metal CuO electrode was lower than for alkaline OER. However, there is still room for further improvement as the anodic potential was significantly higher than the standard potential of MOR to formate. Furthermore, we compared two setups with different characteristics and discussed the implications for the paired synthesis. This work presents the first paired synthesis of methanol oxidation to formate reaching a high formate yield and explicitly investigating the impact of reaction conditions and increasing conversion. Our findings on the effect of conversion, ion balance, and pairing provide valuable insights for further research on methanol oxidation to formate and paired synthesis. In a broader context, our methodology holds potential for investigating electrosynthesis at industrially significant yield and conversion.

CRediT authorship contribution statement

Jonas Baessler: Writing – review & editing, Writing – original draft, Visualization, Methodology, Investigation, Formal analysis, Conceptualization. **Niklas Vollmert:** Writing – review & editing, Writing – original draft, Visualization, Investigation. **Jan Vehrenberg:** Writing – review & editing, Writing – original draft, Methodology. **Miriam Mineur:** Writing – original draft, Visualization, Investigation. **Sophia Schenke:** Visualization, Investigation, Formal analysis. **Lukas Griesberg:** Investigation. **Paulina Montero Pineda:** Investigation. **Robert Keller:** Writing – review & editing, Supervision, Resources, Funding acquisition, Conceptualization.

Declaration of competing interest

The authors declare the following financial interests/personal relationships which may be considered as potential competing interests: Jonas Baessler reports a relationship with FXC Engineering GmbH that includes: board membership, employment, and equity or stocks. Jonas Baessler has patent 'Flusszelle mit verbessertem Aufbau' issued to RWTH Aachen University. Robert Keller has patent 'Flusszelle mit verbessertem Aufbau' issued to RWTH Aachen University. If there are other authors, they declare that they have no known competing financial interests or personal relationships that could have appeared to influence the work reported in this paper.

Data availability

Data will be made available on request.

Declaration of Generative AI and AI-assisted technologies in the writing process

During the preparation of this work, the authors used DeepL (DeepL SE) and ChatGPT (OpenAI LP) in order to improve the language of the manuscript. After using these tools, the authors reviewed and edited the content as needed and take full responsibility for the content of the publication.

Acknowledgments

This work was conducted in part at the Competence Center Industrial Electrochemistry ELECTRA, which is supported by the "European Regional Development Fund (ERDF) and the Federal State of North Rhine-Westphalia, Germany (grant no. ERDF 05 00 07 7). This work was supported by the German Federal Ministry of Education and Research (BMBF) within the project "iNEW2.0" (FKZ 03SF0627). J. Baessler thanks the networking program 'Sustainable Chemical Synthesis 2.0' (SusChemSys 2.0) for the support and fruitful discussions across disciplines. The authors thank Karin Faensen (SEM & EDX), Sandra Gelbach (HPLC), Timo Linzenmeier (HPLC), and Khosrow Rahimi (XRD) for the analytical measurements.

Appendix A. Supplementary data

Supplementary material related to this article can be found online at https://doi.org/10.1016/j.cej.2024.153000.

References

[1] H.-O. Portner, D. Roberts, C. Trisos, N. Simpson, Summary for policymakers: Climate change 2022: Impacts, adaptation, and vulnerability. Contribution of working group II to the sixth assessment report of the intergovernmental panel on climate change, 2022, http://dx.doi.org/10.1017/9781009325844.001.

[2] J. Rissman, C. Bataille, E. Masanet, N. Aden, W.R. Morrow, N. Zhou, N. Elliott, R. Dell, N. Heeren, B. Huckestein, J. Cresko, S.A. Miller, J. Roy, P. Fennell, B. Cremmins, T. Koch Blank, D. Hone, E.D. Williams, S. de La Rue Can, B. Sisson, M. Williams, J. Katzenberger, D. Burtraw, G. Sethi, H. Ping, D. Danielson, H. Lu, T. Lorber, J. Dinkel, J. Helseth, Technologies and policies to decarbonize global industry: Review and assessment of mitigation drivers through 2070, Appl. Energy 266 (2020) 114848, http://dx.doi.org/10.1016/j.apenergy.2020.114848.

[3] J. Wyndorps, H. Ostovari, N. von der Assen, Is electrochemical CO2 reduction the future technology for power-to-chemicals? An environmental comparison with H2-based pathways, Sustain. Energy Fuels 5 (22) (2021) 5748–5761, http://dx.doi.org/10.1039/D1SE00975C.

[4] P. de Luna, C. Hahn, D. Higgins, S.A. Jaffer, T.F. Jaramillo, E.H. Sargent, What would it take for renewably powered electrosynthesis to displace petrochemical processes? Science 364 (6438) (2019) http://dx.doi.org/10.1126/science.aav3506.

[5] S.A. Grigoriev, V.N. Fateev, D.G. Bessarabov, P. Millet, Current status, research trends, and challenges in water electrolysis science and technology, Int. J. Hydrog. Energy 45 (49) (2020) 26036–26058, http://dx.doi.org/10.1016/j.ijhydene.2020.03.109.

[6] M. Jouny, W. Luc, F. Jiao, General techno-economic analysis of CO2 electrolysis systems, Ind. Eng. Chem. Res. 57 (6) (2018) 2165–2177, http://dx.doi.org/10.1021/acs.iecr.7b03514.

[7] J. Na, B. Seo, J. Kim, C.W. Lee, H. Lee, Y.J. Hwang, B.K. Min, D.K. Lee, H.-S. Oh, U. Lee, General technoeconomic analysis for electrochemical coproduction coupling carbon dioxide reduction with organic oxidation, Nat. Commun. 10 (1) (2019) 5193, http://dx.doi.org/10.1038/s41467-019-12744-y.

[8] S. Verma, S. Lu, P.J.A. Kenis, Co-electrolysis of CO2 and glycerol as a pathway to carbon chemicals with improved technoeconomics due to low electricity consumption, Nat. Energy 305 (2019) 968, http://dx.doi.org/10.1038/s41560-019-0374-6.

[9] Á. Vass, B. Endrődi, C. Janáky, Coupling electrochemical carbon dioxide conversion with value-added anode processes: An emerging paradigm, Curr. Opin. Electrochem. 25 (2021) 100621, http://dx.doi.org/10.1016/j.coelec.2020.08.003.

[10] J. Vehrenberg, J. Baessler, A. Decker, R. Keller, M. Wessling, Paired electrochemical synthesis of formate via oxidation of glycerol and reduction of CO2 in a flow cell reactor, 2023, http://dx.doi.org/10.2139/ssrn.4423290.

[11] J. Baessler, T. Oliveira, R. Keller, M. Wessling, Paired electrosynthesis of formic acid from CO2 and formaldehyde from methanol, ACS Sustain. Chem. Eng. 11 (18) (2023) 6822–6828, http://dx.doi.org/10.1021/acssuschemeng.2c07523.

[12] Y. Xu, B. Zhang, Recent advances in electrochemical hydrogen production from water assisted by alternative oxidation reactions, ChemElectroChem 6 (13) (2019) 3214–3226, http://dx.doi.org/10.1002/celc.201900675.

[13] J. Jack, W. Zhu, J.L. Avalos, J. Gong, Z.J. Ren, Anode co-valorization for scalable and sustainable electrolysis, Green Chem. 23 (20) (2021) 7917–7936, http://dx.doi.org/10.1039/D1GC02094C.

[14] Z. Chen, W. Wei, L. Song, B.-J. Ni, Hybrid water electrolysis: A new sustainable avenue for energy-saving hydrogen production, Sustain. Horiz. 1 (2022) 100002, http://dx.doi.org/10.1016/j.horiz.2021.100002.

[15] Formic acid price, 2018, URL: www.intratec.us/chemical-markets/formic-acid-price. (Accessed 09 October 2023).

[16] Methanol price, 2018, URL: www.intratec.us/chemical-markets/methanol-price. (Accessed 09 October 2023).

[17] X. Wei, Y. Li, L. Chen, J. Shi, Formic acid electro-synthesis by concurrent cathodic CO2 reduction and anodic CH3OH oxidation, Angew. Chem. Int. Ed. 60 (6) (2021) 3148–3155, http://dx.doi.org/10.1002/anie.202012066.

[18] J. Hietala, A. Vuori, P. Johnsson, I. Pollari, W. Reutemann, H. Kieczka, Formic acid, in: Ullmann's Encyclopedia of Industrial Chemistry, Vol. 5, Wiley, Chichester, 2010, pp. 1–22, http://dx.doi.org/10.1002/14356007.a12_013.pub3.

[19] D. Wu, J. Hao, Z. Song, X.-Z. Fu, J.-L. Luo, All roads lead to rome: An energy-saving integrated electrocatalytic CO2 reduction system for concurrent value-added formate production, Chem. Eng. J. 412 (2021) 127893, http://dx.doi.org/10.1016/j.cej.2020.127893.

[20] M. Li, X. Deng, Y. Liang, K. Xiang, D. Wu, B. Zhao, H. Yang, J.-L. Luo, X.-Z. Fu, Co_xP@NiCo-LDH heteronanosheet arrays as efficient bifunctional electrocatalysts for co-generation of value-added formate and hydrogen with less-energy consumption, J. Energy Chem. 50 (2020) 314–323, http://dx.doi.org/10.1016/j.jechem.2020.03.050.

[21] M. Li, X. Deng, K. Xiang, Y. Liang, B. Zhao, J. Hao, J.-L. Luo, X.-Z. Fu, Value-added formate production from selective methanol oxidation as anodic reaction to enhance electrochemical hydrogen cogeneration, ChemSusChem 13 (5) (2020) 914–921, http://dx.doi.org/10.1002/cssc.201902921.

[22] K. Xiang, D. Wu, X. Deng, M. Li, S. Chen, P. Hao, X. Guo, J.-L. Luo, X.-Z. Fu, Boosting H2 generation coupled with selective oxidation of methanol into value–added chemical over cobalt hydroxide@hydroxysulfide nanosheets electrocatalysts, Adv. Funct. Mater. 30 (10) (2020) http://dx.doi.org/10.1002/adfm.201909610.

[23] K. Xiang, Z. Song, D. Wu, X. Deng, X. Wang, W. You, Z. Peng, L. Wang, J.-L. Luo, X.-Z. Fu, Bifunctional Pt–Co_3O_4 electrocatalysts for simultaneous generation of hydrogen and formate via energy-saving alkaline seawater/methanol co-electrolysis, J. Mater. Chem. A 9 (10) (2021) 6316–6324, http://dx.doi.org/10.1039/D0TA10501E.

[24] X. Du, M. Tan, T. Wei, H. Kobayashi, J. Song, Z. Peng, H. Zhu, Z. Jin, R. Li, W. Liu, Highly efficient and robust nickel-iron bifunctional catalyst coupling selective methanol oxidation and freshwater/seawater hydrogen evolution via CO-free pathway, Chem. Eng. J. 452 (2023) 139404, http://dx.doi.org/10.1016/j.cej.2022.139404.

[25] M. Ramdin, A.R.T. Morrison, M. de Groen, R. van Haperen, R. de Kler, E. Irtem, A.T. Laitinen, L.J.P. van den Broeke, T. Breugelmans, J.P.M. Trusler, W. de Jong, T.J.H. Vlugt, High-pressure electrochemical reduction of CO2 to formic acid/formate: Effect of pH on the downstream separation process and economics, Ind. Eng. Chem. Res. 58 (51) (2019) 22718–22740, http://dx.doi.org/10.1021/acs.iecr.9b03970.

[26] T.N. Huan, G. Rousse, S. Zanna, I.T. Lucas, X. Xu, N. Menguy, V. Mougel, M. Fontecave, A dendritic nanostructured copper oxide electrocatalyst for the oxygen evolution reaction, Angew. Chem. (Int. ed. Engl.) 56 (17) (2017) 4792–4796, http://dx.doi.org/10.1002/anie.201700388.

[27] T.N. Huan, P. Simon, G. Rousse, I. Génois, V. Artero, M. Fontecave, Porous dendritic copper: An electrocatalyst for highly selective CO2 reduction to formate in water/ionic liquid electrolyte, Chem. Sci. 8 (1) (2017) 742–747, http://dx.doi.org/10.1039/c6sc03194c.

[28] R. Li, J. Xu, R. Zeng, Q. Pan, T. Tang, W. Luo, Halides-assisted electrochemical synthesis of Cu/Cu2O/CuO core-shell electrocatalyst for oxygen evolution reaction, J. Power Sources 457 (2020) 228058, http://dx.doi.org/10.1016/j.jpowsour.2020.228058.

[29] H.A. Miley, Copper oxide films, J. Am. Chem. Soc. 59 (12) (1937) 2626–2629, http://dx.doi.org/10.1021/ja01291a043.

[30] B. Zhang, G. Yang, C. Li, K. Huang, J. Wu, S. Hao, Y. Huang, Electrochemical behaviors of hierarchical copper nano-dendrites in alkaline media, Nano Res. 11 (8) (2018) 4225–4231, http://dx.doi.org/10.1007/s12274-018-2010-3.

[31] M.-I. Jamesh, X. Sun, Recent progress on earth abundant electrocatalysts for oxygen evolution reaction (OER) in alkaline medium to achieve efficient water splitting – A review, J. Power Sources 400 (2018) 31–68, http://dx.doi.org/10.1016/j.jpowsour.2018.07.125.

[32] J. Wang, Y. Gao, H. Kong, J. Kim, S. Choi, F. Ciucci, Y. Hao, S. Yang, Z. Shao, J. Lim, Non-precious-metal catalysts for alkaline water electrolysis: operando characterizations, theoretical calculations, and recent advances, Chem. Soc. Rev. 49 (24) (2020) 9154–9196, http://dx.doi.org/10.1039/d0cs00575d.

[33] H. Heli, M. Jafarian, M.G. Mahjani, F. Gobal, Electro-oxidation of methanol on copper in alkaline solution, Electrochim. Acta 49 (27) (2004) 4999–5006, http://dx.doi.org/10.1016/j.electacta.2004.06.015.

[34] M. Fleischmann, K. Korinek, D. Pletcher, The kinetics and mechanism of the oxidation of amines and alcohols at oxide-covered nickel, silver, copper, and cobalt electrodes, J. Chem. Soc. Perkin Trans. 2 (10) (1972) 1396, http://dx.doi.org/10.1039/p29720001396.

[35] D. Meyerstein, F.M. Hawkridge, T. Kuwana, On the spectroelectrochemical characterization of the electrocatalytic oxidation of Cu(II) ethylenediamine, J. Electroanal. Chem. Interfacial Electrochem. 40 (2) (1972) 377–384, http://dx.doi.org/10.1016/S0022-0728(72)80382-6.

[36] B. Wels, D.C. Johnson, Electrocatalysis of anodic oxygen transfer reactions: Oxidation of cyanide at electrodeposited copper oxide electrodes in alkaline media, J. Electrochem. Soc. 137 (9) (1990) 2785–2791, http://dx.doi.org/10.1149/1.2087072.

[37] V.T.T. Phan, Q.P. Nguyen, B. Wang, I.J. Burgess, Oxygen vacancies alter methanol oxidation pathways on NiOOH, J. Am. Chem. Soc. 146 (7) (2024) 4830–4841, http://dx.doi.org/10.1021/jacs.3c13222.

[38] R.N. Bhatia, K.E. Gubbins, R.D. Walker, Mutual diffusion in concentrated aqueous potassium hydroxide solutions, Trans. Faraday Soc. 64 (1968) 2091, http://dx.doi.org/10.1039/TF9686402091.

[39] S. Parez, G. Guevara-Carrion, H. Hasse, J. Vrabec, Mutual diffusion in the ternary mixture of water + methanol + ethanol and its binary subsystems, Phys. Chem. Chem. Phys. : PCCP 15 (11) (2013) 3985–4001, http://dx.doi.org/10.1039/c3cp43785j.

[40] F.C. Walsh, C. Ponce de León, Progress in electrochemical flow reactors for laboratory and pilot scale processing, Electrochim. Acta 280 (2018) 121–148, http://dx.doi.org/10.1016/j.electacta.2018.05.027.

[41] E. Pérez-Gallent, C. Sánchez-Martínez, L.F.G. Geers, S. Turk, R. Latsuzbaia, E.L.V. Goetheer, Overcoming mass transport limitations in electrochemical reactors with a pulsating flow electrolyzer, Ind. Eng. Chem. Res. 59 (13) (2020) 5648–5656, http://dx.doi.org/10.1021/acs.iecr.9b06925.

[42] P. Cognet, J. Berlan, G. Lacoste, P.-L. Fabre, J.-M. Jud, Application of metallic foams in an electrochemical pulsed flow reactor part I: Mass transfer performance, J. Appl. Electrochem. 25 (12) (1995) http://dx.doi.org/10.1007/BF00242537.

[43] M. Ahmed, I. Dincer, A review on methanol crossover in direct methanol fuel cells: challenges and achievements, Int. J. Energy Res. 35 (14) (2011) 1213–1228, http://dx.doi.org/10.1002/er.1889.

[44] A. Boruń, A. Wypych-Stasiewicz, Conductivity studies of 1:1 electrolytes in water + methanol mixtures at 298.15K, J. Mol. Liq. 344 (2021) 117695, http://dx.doi.org/10.1016/j.molliq.2021.117695.

[45] Y.C. Li, Z. Yan, J. Hitt, R. Wycisk, P.N. Pintauro, T.E. Mallouk, Bipolar membranes inhibit product crossover in CO2 electrolysis cells, Adv. Sustain. Syst. 2 (4) (2018) 1700187, http://dx.doi.org/10.1002/adsu.201700187.

[46] M. Wrobel, S. Kriescher, T. Schiffer, R. Keller, M. Wessling, On the weeping of the GDE cathode during bipolar membrane-based electrochemical CO2 reduction reaction at high current densities, Chem. Eng. J. 474 (2023) 145335, http://dx.doi.org/10.1016/j.cej.2023.145335.

[47] B. Siritanaratkul, M. Forster, F. Greenwell, P.K. Sharma, E.H. Yu, A.J. Cowan, Zero-gap bipolar membrane electrolyzer for carbon dioxide reduction using acid-tolerant molecular electrocatalysts, J. Am. Chem. Soc. 144 (17) (2022) 7551–7556, http://dx.doi.org/10.1021/jacs.1c13024.

[48] K. Xie, R.K. Miao, A. Ozden, S. Liu, Z. Chen, C.-T. Dinh, J.E. Huang, Q. Xu, C.M. Gabardo, G. Lee, J.P. Edwards, C.P. O'Brien, S.W. Boettcher, D. Sinton, E.H. Sargent, Bipolar membrane electrolyzers enable high single-pass CO2 electroreduction to multicarbon products, Nat. Commun. 13 (1) (2022) 3609, http://dx.doi.org/10.1038/s41467-022-31295-3.

[49] R. Pärnamäe, S. Mareev, V. Nikonenko, S. Melnikov, N. Sheldeshov, V. Zabolotskii, H. Hamelers, M. Tedesco, Bipolar membranes: A review on principles, latest developments, and applications, J. Membr. Sci. 617 (2021) 118538, http://dx.doi.org/10.1016/j.memsci.2020.118538.

[50] M. Sassenburg, M. Kelly, S. Subramanian, W.A. Smith, T. Burdyny, Zero-gap electrochemical CO2 reduction cells: Challenges and operational strategies for prevention of salt precipitation, ACS Energy Lett. 8 (1) (2023) 321–331, http://dx.doi.org/10.1021/acsenergylett.2c01885.

[51] J. Balster, R. Sumbharaju, S. Srikantharajah, I. Pünt, D.F. Stamatialis, V. Jordan, M. Wessling, Asymmetric bipolar membrane: A tool to improve product purity, J. Membr. Sci. 287 (2) (2007) 246–256, http://dx.doi.org/10.1016/j.memsci.2006.10.042.

[52] S.Z. Oener, L.P. Twight, G.A. Lindquist, S.W. Boettcher, Thin cation-exchange layers enable high-current-density bipolar membrane electrolyzers via improved water transport, ACS Energy Lett. 6 (1) (2021) 1–8, http://dx.doi.org/10.1021/acsenergylett.0c02078.

[53] G. Xie, T. Okada, Water transport behavior in nafion 117 membranes, J. Electrochem. Soc. 142 (9) (1995) 3057–3062, http://dx.doi.org/10.1149/1.2048686.

[54] A. Zlotorowicz, R.V. Strand, O.S. Burheim, Ø. Wilhelmsen, S. Kjelstrup, The permselectivity and water transference number of ion exchange membranes in reverse electrodialysis, J. Membr. Sci. 523 (2017) 402–408, http://dx.doi.org/10.1016/j.memsci.2016.10.003.

[55] S.B. Solberg, P. Zimmermann, Ø. Wilhelmsen, R. Bock, O.S. Burheim, Analytical treatment of ion-exchange permselectivity and transport number measurements for high accuracy, J. Membr. Sci. 685 (2023) 121904, http://dx.doi.org/10.1016/j.memsci.2023.121904.